# HEIGHT RETRIEVAL OF ISOLATED BUILDINGS

# FROM SINGLE HIGH RESOLUTION SAR IMAGES

Raffaella Guida[1], *IEEE Member*, Antonio Iodice[2], *IEEE Senior Member*,
Daniele Riccio[2], *IEEE Senior Member*.


[1] Surrey Space Centre
University of Surrey
Guildford, Surrey
Tel. +(44) (0)1483 682227, fax +(44) (0)1483 689503
E-mail: R.Guida@surrey.ac.uk

[2] Dipartimento di Ingegneria Biomedica, Elettronica e delle Telecomunicazioni,
Università di Napoli Federico II
Via Claudio 21, 80125 Napoli, Italy.
Tel. +(39)-0817683114, fax +(39)-0815934448
E-mail: {iodice, Daniele.Riccio}@unina.it

## Abstract

Detection of man-made structures in urban areas, in terms of both geometric and electromagnetic features, from a single, possibly High Resolution (HR), Synthetic Aperture Radar (SAR) image is a highly interesting open challenge. Within this framework a possible approach for the extraction of some relevant parameters, describing shape and materials of a generic building, is here proposed. The approach is based on sound electromagnetic models for the radar returns of each element of the urban scene: a fully analytical representation of electromagnetic returns from the scene constituents to an active microwave sensor is employed. Some possible applications of feature extractions from real SAR images, based on above approach, have been already presented in literature as first examples of potentiality of a model-based approach but here the overall theory is analyzed and discussed in depth, to move to general considerations about its soundness and applicability, as well as efficiency of further applications may be derived.

For the sake of conciseness, although the proposed approach is general and can be applied for the retrieval of different scene parameters (in principle, anyone contributing to the radar return),

we here focus on the extraction of the building height, and we assume that the other parameters are either *a priori* known (e.g., electromagnetic properties of the materials), or have been previously retrieved from the same SAR image (e.g., building length and width). An analysis of the sensitiveness of the height retrieval to both model inaccuracies and to errors on the knowledge of the other parameters is performed. Some simulation examples accompany and validate the solution scheme that we propose.

## I. Introduction

Nowadays, the remote sensing scientific community is continuously increasing its efforts in the field of information extraction from remote sensing data relative to urban scenes.

The attempt to retrieve information from Synthetic Aperture Radar (SAR) images seems to be promising in comparison with other remote sensing data [1-3]: this is mainly due to the SAR aptitude to acquire high-resolution, all-weather, illumination-independent data. The use of different SAR technologies has been explored, including airborne and spaceborne sensors, new operational modes, and configurations (e.g., SAR interferometry): some results relevant to the information extraction from SAR images can be found in the literature [1-2, 4-20]. Some studies, e.g., [6,7,9,13], tried to exploit SAR interferometry in feature retrieval when built-up areas are considered. However, this technique may fail, for instance in the phase unwrapping, because radar data from urban areas are always affected by layover and shadowing effects.

Availability of many SAR datasets has stimulated researchers in the attempt of improving the urban area characterization (e.g., via the description of road networks or classification of land cover classes) by using multitemporal and/or multiangle (or multibaseline) SAR images [5,16]. In other cases, airborne SAR images, stereoscopic [17] or multi-aspect meter-resolution [18], have been employed for the 3-D reconstruction of buildings.

Conversely only very few papers, dealing with building reconstruction from a single High-Resolution (HR) SAR image of urban scenes, can be found in literature [8,11,19,20]. These papers

introduce quite new, rough approaches which are very promising in terms of sensitiveness to the high complexity of urban scenes; but in these cases only simple and rough estimations have been performed, mostly concerning only with some geometric parameters as building height, shape or position [8,11,19]. Within this framework a pattern recognition, for instance in the case of roads extraction from the SAR image, can be reached by a hierarchical approach: thematic classes in the SAR image are iteratively individuated by considering radiometric and geometric properties [20]. Moreover, continuous changes in urban scenarios lead to solve the problem of feature extraction from a dynamic environment. In this case, use of some artificial neural networks have been proposed for their ability to deal with temporal changes in the urban area features and corresponding SAR image complexity, [4]. For most of the mentioned works, a stochastic analysis provides a compulsory step to deal with the high complexity exhibited by SAR images of urban scenes.

However, an alternative deterministic approach, able to invert geometric and electromagnetic models, can be conceived. Till few years ago, this was a hard task due to the lack of physical and mathematical models able to describe the complex interactions among the radar signal and the man made objects in the scene. In [21-22], a first attempt in this direction was made: first, a direct backscattering model for an isolated element of an urban scene was presented in [21]; this backscattering model was then included in a SAR raw signal simulator for urban structures [22]. Availability of such a simulation tool is a fundamental support in developing the idea of a deterministic extraction of geometric and electromagnetic parameters from HR SAR images [14]. The backscattering model and the SAR simulator provide a full (analytical and numerical) set of direct relationships between the parameters of each building of the urban area and some measurable parameters in the corresponding SAR images: all this material provides the background for the inverse problem that we propose to solve via a deterministic approach.

The basic idea, whose guidelines were briefly introduced in a form of a draft in [14], is now developed in detail, discussed and finally validated on simulated images. Note that here we do not

consider the preliminary step of automatic building detection (in fact, a manual detection is performed in the provided examples), but we rather focus on the parameter inversion step. In any case our manual approach is based on new direct models mostly developed in closed form for the direct problem: thus, it could be conceived as the first step to generate a new retrieval technique that is eligible for a mature application whenever inserted in an automatic approach.

In Section II, we define a set of geometric and radiometric parameters measurable on a SAR image of isolated buildings (i.e., sizes of layover and shadow areas, orientation angle of the building, radar cross section), and a set of geometric and electromagnetic scene parameters to be estimated (i.e., height, length and width of the building; complex dielectric constants of walls, roof and soil; soil roughness parameters). Then, in Section III we obtain a set of analytical expressions that link the parameters to be estimated to the measured ones. The obtained relationships allow writing a set of independent equations which can be solved by using a least square approach. In Section IV we restrict our attention to the building height retrieval, and we assume that the other parameters are either *a priori* known (i.e, complex dielectric constants of walls, roof and soil; soil roughness parameters), or have been previously retrieved from the same SAR image (i.e., building length, width and orientation angle). The retrieval algorithm is then described in detail. In Section V we perform an analysis of the sensitiveness of the height retrieval to both model inaccuracies and errors on the knowledge of the other parameters. In Section VI some examples of building height retrieval from simulated SAR images (for which the "ground truth" is perfectly known) are presented in order to assess the accuracy of the retrieval scheme. Finally, in Section VII some concluding remarks are reported and future perspectives are briefly introduced.

## II. Statement of the problem

SAR images relevant to urban centres can be very difficult to be understood and complicated to be interpreted. This is due not only to the presence of some distortion effects usually emphasized in similar frameworks (like shadow and layover [23]) but, above all, to the increase of

multiple scattering when man-made objects crowd the scene under detection. In fact, contributions relevant to different buildings may partially overlap each other, so that the radar return from each building is mixed with returns from surrounding structures.

In the following we refer to a scene composed by isolated buildings placed on a rough terrain. Terrain roughness is here modelled by a Gaussian stochastic process with Gaussian autocorrelation function. Each building in the scene is isolated in a radar sense: its radar returns do not interfere with any return from other buildings in the scene. This case is a very useful canonical scene: it provides a simplified view that can nicely fit only some particular actual scenes, but it represents a preliminary compulsory step to be approached to solve the problem of a deterministic feature extraction from a single amplitude SAR image.

To simplify the problem, we proceed as in [21] by modelling the building via a parallelepiped with flat surfaces, see Fig.1. This implies that we do not consider the presence (and then the corresponding contribution to the SAR image) of windows and balconies and we consider flat roofs. The effects of these simplifying assumptions are analysed in Section V, where they are relaxed and a more realistic shape for modelling the building is considered.

Now, we can define a finite set of *geometric* parameters to be estimated for the building and the surrounding soil:

- Building height $h$;

- Building length $l$;

- Building width $w$;

- Roughness parameters, i.e., the standard deviation $\sigma$ and the correlation length $L$ of the Gaussian stochastic process describing the soil surface profile.

In the same way, let us define a set of *electromagnetic* parameters to be estimated for the building and the surrounding soil:

- The complex dielectric constant of the walls $\varepsilon_w$;

- The complex dielectric constant of the roof $\varepsilon_r$;

- The complex dielectric constant of the soil $\varepsilon_s$.

The above lists of parameters represent the geometric and electromagnetic information that we propose to extract from a single high resolution SAR image (*retrievable parameters*). These cannot be directly measured on a SAR image of the building. So we need to define also a set of geometric and electromagnetic parameters that are directly measurable on SAR images. To this aim, it is useful to describe how radar returns from different parts of the building are mapped on the SAR image, due to the fact that they reach the receiver at different times. For a complete detailed description, the reader is referred to, e.g., [22]. We here recall that, as illustrated in Fig.2, by proceeding on the SAR image at constant azimuth and from near to far range, we first find a bright stripe corresponding to the superposition of backscattering from ground, wall and roof (i.e., to *layover* [23]); then a (usually very) bright line corresponding to wall-ground and ground-wall double scattering (indeed double scattering ray paths all have the same length, see [22]); then a grey area corresponding to backscattering from roof (this area may disappear for very tall buildings, see Fig.2); and finally a dark area corresponding to the building *shadow* [23]. Higher order multiple scattering (in particular, triple scattering, see Fig.2 and Section III) may occur, but it is usually negligible with respect to other contributions. Based on these considerations, the geometric and electromagnetic parameters that are directly measurable on SAR images are:

- the range dimensions of layover and shadow areas, $L_r$ and $S_r$ in Fig.2, relevant to the considered building;

- the angle $\varphi$ between the sensor line of flight and the projection of a wall of the building to the ground;

- the radar cross sections of layover area, double scattering line, and, if applicable, backscattering from roof, pertinent to the considered building.

Obviously, this last set of parameters (*measurable parameters*) is strictly linked to the first two, and in fact a set of analytical expressions relating the *retrievable* parameters to the *measurable* ones can be found, as shown in Section III.

### III. General retrieval approach

This section is divided into two parts: in the first one, by collecting and developing results available in literature, we find analytical expressions linking the *retrievable* parameters to the *measurable* ones (direct problem); in the second part we describe a general procedure for the extraction of the *retrievable* parameters from the *measurable* ones (inverse problem).

As far as the direct problem is under concern, we can distinguish between relationships that only involve geometric parameters and relationships that also involve radiometric (i.e., electromagnetic) parameters. The former can be obtained by considering the simple building geometrical model depicted in Section II and by measuring some relevant lengths on the corresponding SAR image. As a matter of fact, Fig.2 shows that range sizes of layover, $L_r$, and shadow, $S_r$, are linearly linked to the height $h$ of the considered building via the SAR look angle $\vartheta$; this link still exists if the wall is not aligned with the sensor flight trajectory. Procedures proposed in [11-13,19] are based on this observation.

We can then derive the following relationships [11],[24]:

$$\circ \quad h = \frac{L_r}{\cos \vartheta} \tag{3.1}$$

$$\circ \quad h = S_r \cos \vartheta \quad ; \tag{3.2}$$

Note that both equations are applicable if $\vartheta > \vartheta_p = \tan^{-1}\left(\dfrac{h}{w}\right)$, see Fig.2 top; conversely, for

$\vartheta < \vartheta_p = \tan^{-1}\left(\dfrac{h}{w}\right)$, see Fig.2 down, layover partly masks shadow, then eq.(3.2) is not applicable

and $h$ can be extracted only from $L_r$ via eq.(3.1). Note also that eq.(3.2) assumes that terrain surrounding the building is horizontal (i.e., no slope is present), as it is usually the case.

Other geometrical relations, involving the building length $l$ and width $w$, can be obtained by observing Fig.3. As a matter of fact $l$ (or $w$) can be also extracted from geometric parameters by

measuring, on the azimuth-slant range SAR image, the distances $dx$ and $dr$ that are shown in Fig.3; these measurable quantities are linked to $l$ through the following expressions:

$$dy = \frac{dr}{\sin \vartheta},$$ (3.3)

$$l = \sqrt{dx^2 + dy^2} .$$ (3.4)

Analogous relations can be obtained for $w$ by considering the other illuminated building wall. In a different way, as shown in [11], $w$ can be also extracted by measuring, depending on the situations, either the range lengths $X$ or $S_r$; by considering the quantities represented in Fig.2 we get:

- $w = \dfrac{X}{\sin \vartheta} \cos \varphi$       if     $\vartheta > \vartheta_p = tg^{-1}\left(\dfrac{h}{w}\right)$ (3.5)

- $w = \left[\dfrac{S_r}{\sin \vartheta} - h \tan \vartheta\right] \cos \varphi$      if     $\vartheta < \vartheta_p = tg^{-1}\left(\dfrac{h}{w}\right)$ (3.6)

Obviously, for $\varphi$ different from zero (note that $\varphi$ is estimated with an accuracy depending on the building orientation and dimensions) the roles of $l$ and $w$ are interchangeable, so that (3.3-4) and (3.5-6) can be written for both $l$ and $w$ but each couple of equations above obviously allows extraction with different precision according to the radar geometry; conversely, for the case of $\varphi$ equal to zero (3.5-6) can only be used for $w$.

Let us now consider the relations involving also the electromagnetic parameters. To this aim, a sound electromagnetic model, able to describe the radar return from the canonical structure in Fig.1, is required. Numerical electromagnetic methods may provide precise evaluations for the field scattered from a specific building; however, we prefer considering analytical electromagnetic methods because we need to fully explore the functional dependence between the scattered

electromagnetic field and the scene parameters. As a matter of fact, in [21] analytical expressions of the radar cross section $\sigma^o$ of a building modelled as a smooth parallelepiped on a possibly rough terrain are provided. More specifically, the radar return from such a structure is decomposed into single scattering contributions from the (rough) ground, the building roof (a plane surface in our model), the vertical (smooth) walls and multiple scattering contributions from dihedral structures formed by vertical walls with the ground (see Fig.1). Single scattering contributions are evaluated by using the Kirchhoff Approach (KA), in the Physical Optics (PO) or Geometrical Optics (GO) approximations according to the ground roughness [21]. In order to account for multiple scattering between buildings and terrain, the GO is used to evaluate the field reflected by the smooth wall toward the ground (first bounce) or the sensors (second or third bounce), and KA to evaluate the field scattered by the rough ground toward the wall (first or second bounce) or the sensors (second bounce), again by employing the PO or GO approximations according to the ground roughness. Among multiple scattering contributions, only double and triple scattering are considered, because higher order contributions are not present if the wall surface is supposed to be smooth and GO is used to evaluate the field that it reflects [21]. Accordingly, Ref.[21] provides the expressions for: PO and GO single scattering from ground, wall and roof; GO-PO and GO-GO wall-ground (or ground-wall) double scattering; GO-PO-GO and GO-GO-GO wall-ground-wall triple scattering. Note that different contributions reach the receiver at different times, so that they appear at different range coordinates in the SAR image, as already discussed in Section II.

All the analytical expressions provided in [21] can be used in the general retrieval scheme we here propose. For the sake of conciseness, we hereafter report only the double scattering expressions involving the building height $h$, because they are used in the next Section:

$$\sigma^\circ = h \cdot f(\mathbf{p}) \quad , \tag{3.7}$$

where $\mathbf{p}$ is a vector of known parameters: $\mathbf{p} = (l,\ \sigma,\ L,\ \varepsilon_w,\ \varepsilon_s,\ \varphi,\ \vartheta)$; and $f(\mathbf{p})$ is given by either

$$f(\mathbf{p}) = \left|S_{pq}\right|^2 l \tan\vartheta\cos\varphi\exp\left(-4k^2\sigma^2\cos^2\vartheta\right)\sum_{m=1}^{\infty}\frac{\left(2k\sigma\cos\vartheta\right)^{2m}}{m!}\frac{k^2L^2}{4m}\exp\left[-\frac{\left(2kL\sin\varphi\sin\vartheta\right)^2}{4m}\right]$$

(3.8)

if GO-PO solution is considered for the double scattering incoherent radar cross section $\sigma^o$, or

$$f(\mathbf{p}) = \frac{\left|S_{pq}\right|^2 l \tan\vartheta\cos\varphi\left(1+\tan^2\vartheta\sin^2\varphi\right)\cdot\exp\left[-\frac{\tan^2\vartheta\sin^2\varphi}{2\sigma^2\left(2/L^2\right)}\right]}{8\pi^2\cos^2\vartheta\cdot\sigma^2\left(2/L^2\right)}$$

(3.9)

when GO-GO solution is assumed for the double scattering radar cross section $\sigma^o$.

In eqs.(3.8-9), $S_{pq}$, with $p$ and $q$ each standing for $h$ or $v$ (horizontal or vertical polarization), is the generic element of scattering matrix, see [21], which is dependent on the dielectric constants of wall and soil, and on look and orientation angles and $k=2\pi/\lambda$ is the wavenumber.

In conclusion, key qualitative comments to the above cited quantitative relationships between measurable and retrievable parameters are summarized in Tables I and II. These comments are included to support the possible use of the above mentioned relationships in the retrieval procedure.

Relations (3.1-9), and the other radar cross section expressions provided in [21], can be organised in a system of independent equations in the unknowns $h$, $l$, $w$, $\sigma$, $L$, $\varepsilon_w$, $\varepsilon_s$, (or only some of these, if the others are known) which can be solved for instance by using a least square approach [25].

Above considerations lead now to define the following general retrieval procedure: given a set of parameters to be retrieved,

STEP 1: Measure some relevant parameters on the SAR image (measurable parameters, i.e., layover and shadow sizes, lengths $dx$ and $dr$, angle $\varphi$, radar cross sections of different contributions that map on different parts of the image).

STEP 2: Choose the proper analytical relations, among the available ones linking retrievable and measurable parameters, in order to write a system of equations whose unknowns are the parameters to be retrieved.

STEP 3: Solve the system of equations in the least square sense.

Obviously, this general procedure needs to be better specified for each parameter or set of parameters to be retrieved. In the following of the paper, to fully show the proposed procedure implications and peculiarities, we focus our attention on the retrieval of the building height.


## IV. Building height retrieval procedure

In this Section we focus on the retrieval of the building height, and we assume that the other parameters are either *a priori* known (i.e, complex dielectric constants of walls, roof and soil; soil roughness parameters), or have been previously retrieved from the same SAR image (i.e., building length and width, orientation angle). Of course, extension to the simultaneous inversion of multiple parameters is conceptually possible if the number of unknown parameters is smaller than or equal to the number of available equations. In practice, this extension is straightforward as long as only linear equations are involved, as in the case of the retrieval of $h$, $l$, $w$. Conversely, simultaneous retrieval of soil roughness parameters and dielectric constants of materials leads to non-linear systems of equations, for which a least square solution may be difficult to obtain due to the appearance of multiple minima. In this case, more sophisticated, or *ad hoc* (see e.g.[1]), methods must be used.

The building height $h$ appears both in the geometrical relations (3.1-2) and in the radar cross section expressions of [21] for single scattering from wall, double scattering, and triple scattering. However, single scattering from wall is always overlapped and masked by single scattering from

the rough ground and from the roof in the layover area (see Fig.2 and Section II), so that it is not possible to distinguish this contribution from the others. Similarly, the triple scattering is always very weak and is often overlapped by other stronger contributions, so that it is very hard to be distinguished. Conversely, the double scattering line (at least if the angle $\varphi$ is not large) is bright and easily distinguishable. Accordingly, we propose to use the radar cross section of this contribution to retrieve the building height, and to this aim we can use eq.(3.8) for low soil roughness (and $\varphi$ different from zero, otherwise a coherent component should be added to (3.8), see [21]), or eq.(3.9) for high soil roughness.

### 4.1. STEP 1. Measurements on the SAR image

Based on the above considerations, for the case at hand the STEP 1 of the previously defined procedure consists of the measurement of layover and shadow areas range sizes and of the radar cross section of the double scattering bright line. This requires a preliminary segmentation step to identify, in the SAR image, layover, shadow and double scattering areas relevant to the buildings under investigation. We use a simple supervised segmentation based on a threshold on pixel grey levels. The choice of the threshold is performed via the histogram method [26]. However, more sophisticated segmentation methods could be used [26]. Once layover and shadow areas have been identified, their range sizes are measured by a simple pixel count (obviously, SAR image pixel spacing is known). Similarly, once the double scattering bright line has been identified, the corresponding radar cross section is obtained by averaging the grey level values over the pixels belonging to the line. This average reduces the speckle noise: it is a spatial multilook operation, possibly with a large number of looks [23]. In the following examples, the average is carried out on the amplitude image so the measured value is linked to the square root of the radar cross section but the same operation could be performed also on the power image provided that the right relationships are then considered in the next steps.

All these measures, whether geometric or radiometric, are performed manually with the support of software for image processing. Interactive Data Language (IDL) has been adopted for the examples shown in the next sections.

### 4.2. STEP 2: Obtaining a system of equations

With regard to STEP 2, as already noted eqs.(3.1), (3.2) and (3.7), can be used. The use of eqs.(3.1-2) is straightforward, whereas the use of eq.(3.7) requires some discussion about radiometric calibration. In fact, if we use a radiometrically calibrated SAR image, then the relationship between grey levels and the radar cross section is known. If this is not the case, a multiplicative unknown constant, due to unknown attenuation, and an additive unknown constant, due to the background noise, must be added to the radar cross section in eq.(3.7). These two unknown constants can be computed from eq.(3.7) itself if the heights of at least two buildings in the scene (we call them *calibrating buildings*) are known. The computation of these unknown constants will be referred to as "calibration operation" in the following and is detailed in Appendix A. In the simplifying (but often satisfied in bright areas of SAR images) assumption that the additive constant is negligible, it turns out that only a single calibrating building is needed, and the building height can be evaluated as (see Appendix A):

$$ h = h_c \frac{\hat{\sigma}^o}{\hat{\sigma}_c^o} \frac{f(\mathbf{p}_c)}{f(\mathbf{p})} \quad , \tag{4.1} $$

where $h_c$ is the known height of the "calibrating" building, $\hat{\sigma}^o$ and $\hat{\sigma}_c^o$ are the measured radar cross sections (i.e., the square of the SAR amplitude image grey level) of examined and "calibrating" buildings, respectively, and, similarly, $\mathbf{p}$ and $\mathbf{p}_c$ are the known parameters relative to the examined and "calibrating" buildings, respectively. As shown in Section V, this calibration operation may be useful even when a radiometrically calibrated SAR image is available, because it avoids the effects

of radiometric calibration errors and reduces the sensitiveness to errors on knowledge of parameters and to inaccuracies of the electromagnetic model.

### 4.3. STEP-3: Solving the system of equations

The solution of the system of equations (3.1), (3.2), and either (3.7) or (4.1) is now in order. This is a simple *linear* system of three equations in the *single* unknown $h$. Independency of the three equations is guaranteed by the independent measurement errors affecting their known terms. It is easy to verify that in this case the least square solution of the system, i.e., STEP 3 of the previously defined procedure, can be evaluated as:

$$h = \sum_{i=1}^{N} a_i h_i \quad , \tag{4.2}$$

where $N=3$ for the case at hand, $h_i$ is the solution of the $i$-th equation of the system, $a_i$ is the appropriate weight for the $i$-th equation, and $\sum_{i=1}^{N} a_i = 1$ . Of course, use of eq.(4.2) requires a proper choice of the weights $a_i$, and this can be achieved only if we know the accuracy of the height $h_i$ obtained from the $i$-th equation and if $h_i$ can be modelled as independent Gaussian random variables (in fact, if $h_i$ are independent Gaussian random variables with variances proportional to $a_i$, then the least square solution coincides with the maximum likelihood one). If this information is not available, the weights can be chosen all equal (in the case at hand, all equal to 1/3).

Some information on accuracy of the determinations of $h_i$ from eqs.(3.1-2), (3.7) and (4.1) can be obtained from the theoretical analysis performed in the next Section, and from the simulation-based results reported in Section VI. However, in the choice of weights $a_i$, these results should be integrated by a priori knowledge on uncertainty sources and on their possible cross-correlations, which are impossible to predict in the general case. Therefore, in the next Sections we do not discuss this issue in detail.

**V. Height retrieval accuracy**

In this Section the accuracy of the height retrieval from eqs.(3.1-2) and (4.1) is analysed. The error sources for the retrieval procedure are the inaccuracy of the employed geometric and electromagnetic model, and the uncertainty on the knowledge of the parameters appearing in eqs.(3.1-2) and (4.1). We first consider the latter.

*5.1 Uncertainty on input parameters: analytical evaluation*

With regard to eq.(3.1), it is evident that the uncertainty $\Delta h$ on the retrieved value of $h$ is $1/\cos\vartheta$ times the uncertainty on the size $L_r$ of layover area. Since the latter is of the order of the SAR slant range resolution $R$, then we get that $\Delta h$ is of the order of $R$:

$$\Delta h = \frac{R}{\cos\vartheta} \qquad \Rightarrow \qquad \frac{\Delta h}{h} = \frac{R}{h} \cdot \frac{1}{\cos\vartheta} \qquad . \tag{5.1}$$

Similarly, with regard to eq.(3.2), the uncertainty $\Delta h$ on the retrieved value of $h$ is $\cos\vartheta$ times the uncertainty on the size $S_r$ of shadow area, so that also in this case the uncertainty on the retrieved value of $h$ is of the order of $R$, but it is smaller with respect to the previous case, because $\cos\vartheta < 1/\cos\vartheta$:

$$\Delta h = R\cos\vartheta \qquad \Rightarrow \qquad \frac{\Delta h}{h} = \frac{R}{h}\cos\vartheta \qquad . \tag{5.2}$$

We are assuming that the look angle $\vartheta$ is perfectly known (as it is usually the case), so that we do not consider the effect of uncertainty on the value of $\vartheta$.

Let us now consider eq.(4.1). In this case the sources of errors are the uncertainties on $h_c$, $\hat{\sigma}^o$, $\hat{\sigma}_c^o$, **p** and **p**$_c$. The uncertainty $\Delta h$ on the retrieved value of $h$, caused by an uncertainty $\Delta h_c$ on $h_c$, is

$$\Delta h = \left| \frac{\partial h}{\partial h_c} \right| \Delta h_c = \frac{h}{h_c} \Delta h_c \qquad \Rightarrow \qquad \frac{\Delta h}{h} = \frac{\Delta h_c}{h_c} \quad , \tag{5.3}$$

and we get that the relative uncertainty on $h$ is equal to the relative uncertainty on $h_c$.

With regard to the uncertainties $\Delta \hat{\sigma}^o$ and $\Delta \hat{\sigma}_c^o$ on the measured radar cross sections $\hat{\sigma}^o$ and $\hat{\sigma}_c^o$, we underline that they are only related to the presence of speckle noise, and not to absolute calibration errors, which are cancelled out in the ratio $\hat{\sigma}^o / \hat{\sigma}_c^o$. In the worst case of fully developed speckle [23], we have that $\Delta \hat{\sigma}^o = \hat{\sigma}^o / \sqrt{N}$ and $\Delta \hat{\sigma}_c^o = \hat{\sigma}_c^o / \sqrt{N_c}$, where $N$ and $N_c$ are the number of looks (i.e., the number of independent samples averaged to measure the radar cross section). In the case at hand, in which the radar cross section is estimated by averaging over the entire double reflection line, $N$ is the number of resolution cells in the double reflection line, i.e., $N = l/R$, where $l$ is the building length and $R$ is the SAR image resolution. Similarly, $N_c = l_c/R$, where $l_c$ is the calibrating building length. Accordingly, we have that the uncertainty $\Delta h$ on the retrieved value of $h$, caused by an uncertainty $\Delta \hat{\sigma}^o$ on $\hat{\sigma}^o$, is equal to:

$$\Delta h = \left| \frac{\partial h}{\partial \hat{\sigma}^o} \right| \Delta \hat{\sigma}^o = \frac{h}{\hat{\sigma}^o} \Delta \hat{\sigma}^o \leq \frac{h}{\sqrt{N}} = h \sqrt{\frac{R}{l}} \qquad \Rightarrow \qquad \frac{\Delta h}{h} \leq \sqrt{\frac{R}{l}} \quad . \tag{5.4}$$

Similarly, the uncertainty $\Delta h$ on the retrieved value of $h$, caused by an uncertainty $\Delta \hat{\sigma}_c^o$ on $\hat{\sigma}_c^o$, is given by:

$$\Delta h = \left| \frac{\partial h}{\partial \hat{\sigma}_c^o} \right| \Delta \hat{\sigma}_c^o = \frac{h}{\hat{\sigma}_c^o} \Delta \hat{\sigma}_c^o \leq \frac{h}{\sqrt{N_c}} = h \sqrt{\frac{R}{l_c}} \quad \Rightarrow \quad \frac{\Delta h}{h} \leq \sqrt{\frac{R}{l_c}} \quad . \tag{5.5}$$

Let us now consider the parameters constituting $\mathbf{p}$ as source of error on $f(\cdot)$. First of all we note that if the parameters are the same for both the examined and the calibrating building ($\mathbf{p}=\mathbf{p}_c$), they do not affect the retrieved height, because their effects are cancelled out in the calibration operation, see (4.1). This is not a completely unrealistic situation if the two buildings are in the same neighbourhood. However, in the following we consider the more general case in which $\mathbf{p}$ is different from $\mathbf{p}_c$.

The uncertainty $\Delta h$ on the retrieved value of $h$, caused by an uncertainty $\Delta l$ on $l$, is

$$\Delta h = \left| \frac{\partial h}{\partial f} \right| \left| \frac{\partial f}{\partial l} \right| \Delta l = h_c \frac{\hat{\sigma}^o}{\hat{\sigma}_c^o} \frac{f(\mathbf{p}_c)}{f^2(\mathbf{p})} \left| \frac{\partial f}{\partial l} \right| \Delta l = \frac{h}{f(\mathbf{p})} \frac{f(\mathbf{p})}{l} \Delta l \quad \Rightarrow \frac{\Delta h}{h} = \frac{\Delta l}{l} \quad . \tag{5.6}$$

Note that for high resolution sensor the building length $l$ is larger than the sensor resolution: if this is the case, in the above formulas $l$ must be meant as the length of the portion of the building belonging to a resolution cell (i.e., R/cos($\varphi$), for $\varphi$ not too large).

A similar procedure can be used for soil roughness parameters. We here consider the GO-GO solution, eq.(3.9). In this case, the double scattering contribution depends on the two roughness parameters only via the root mean square slope $s_{rms} = \frac{\sqrt{2}\sigma}{L}$. Accordingly, we can evaluate the uncertainty $\Delta h$ on the retrieved value of $h$, caused by an uncertainty $\Delta s_{rms}$ on $s_{rms}$:

$$\Delta h = \left| \frac{\partial h}{\partial f} \right| \left| \frac{\partial f}{\partial s_{rms}} \right| \Delta s_{rms} = h_c \frac{\hat{\sigma}^o}{\hat{\sigma}_c^o} \frac{f(\mathbf{p}_c)}{f^2(\mathbf{p})} \left| \frac{\partial f}{\partial s_{rms}} \right| \Delta s_{rms} = \frac{h}{f(\mathbf{p})} \frac{f(\mathbf{p})}{s_{rms}} \left| -2 + \frac{\sin^2 \varphi \tan^2 \vartheta}{s_{rms}^2} \right| \Delta s_{rms}$$

$$\Rightarrow \quad \frac{\Delta h}{h} = \frac{\Delta s_{rms}}{s_{rms}} \left| -2 + \frac{L^2 \sin^2 \varphi \tan^2 \vartheta}{s_{rms}^2} \right| \approx \frac{\Delta s_{rms}}{s_{rms}} \quad . \tag{5.7}$$

This equation is obtained by assuming that the roughness of the soil surrounding the examined building is affected by an uncertainty $\Delta s_{rms}$, whereas the roughness of the soil surrounding the calibrating building is perfectly known and, in general, different from the former. However, in some realistic situations, the roughness is the same for both soils, and the error on its assumed value is also the same. In this case, see Appendix B, the height relative error is

$$\frac{\Delta h}{h} = \exp \left\{ -\frac{\tan^2 \vartheta}{2} \left[ \frac{1}{\left( s_{rms} + \Delta s_{rms} \right)^2} - \frac{1}{s_{rms}^2} \right] \left[ \sin^2 \varphi_c - \sin^2 \varphi \right] \right\} - 1 \cong$$
$$\cong \frac{\tan^2 \vartheta}{s_{rms}^2} \left( \sin^2 \varphi - \sin^2 \varphi_c \right) \frac{\Delta s_{rms}}{s_{rms}} \tag{5.8}$$

Eq.(5.8) shows that if the examined and calibrating buildings are aligned (for instance, if they are on the same straight street), an error on the soil roughness has no effect on the retrieved height.

### 5.2 Uncertainty on input parameters: numerical analysis

For uncertainties on the dielectric constants and on the orientation angle, a simple analytical study is not possible. More precisely, even if the relative derivatives can be still computed, they result to be so involved that poor considerations can be carried on about the influence on height estimation. For this reason, the analytical expressions in closed-form of the errors have been computed with the support of a computer code but we here prefer to report the graphical representation of the result which has been preferred to the analytical one, allowing more useful considerations.

Again, considering the uncertainty on the orientation angle $\varphi$, it can be written as

$$\frac{\Delta h}{h} = \frac{1}{f(\mathbf{p})}\left|\frac{\partial f}{\partial \varphi}\right|\Delta\varphi = \frac{\varphi}{f(\mathbf{p})}\left|\frac{\partial f}{\partial \varphi}\right|\frac{\Delta\varphi}{\varphi}$$

(5.9)

and the function $\dfrac{\varphi}{f(\mathbf{p})}\left|\dfrac{\partial f}{\partial \varphi}\right|$ is plotted at variance of $\varphi$ for different polarizations in Fig.4. Here and

in the following this function is called *error propagation factor*, being the ratio between the relative

uncertainty on $h$ and the relative uncertainty on the unknown parameter. In case of a large error

propagation factor, even a small uncertainty on the unknown parameter may cause a large

uncertainty on $h$. In Fig.4, as in the simulation examples, we adopted the scene parameters listed in

Table III while for the radar look angle $\theta$ the value of 30 degrees has been assumed.

According to the plots in Fig.4, all polarizations present their worst case for $\varphi$ approaching

$\pi/2$. In this case, in fact, even a minimal inaccuracy on the knowledge of the wall orientation

strongly affects the height retrieval. However, in case of buildings whose shape is modelled with a

parallelepiped, for any wall oriented quite perpendicular to the radar trajectory, there exists another

wall that is basically parallel to the radar trajectory and that must be preferred for the height

retrieval by double reflection for its stronger contribution.

Anyway, an error on $\varphi$ seems to deeply affect the height evaluation but, fortunately, the

building orientation angle can be in general extracted from the radar image with a very good

accuracy; moreover, by considering high resolution SAR, this measurement error on $\varphi$ is smaller.

As far as the dielectric constant is under concern, we model it via the corresponding

permittivity and conductivity; the analysis of the influence of this parameter is divided in two parts:

the permittivity is supposed unknown in the first one and the conductivity in the second.

But a general expression can be derived for the relative error, *Δh/h*. The uncertainty on the

permittivity/conductivity of either the wall or the ground is

$$\frac{\Delta h}{h} = \frac{1}{f(\mathbf{p})}\left|\frac{\partial f}{\partial \varepsilon_x}\right|\Delta\varepsilon_x = \frac{\varepsilon_x}{f(\mathbf{p})}\left|\frac{\partial f}{\partial \varepsilon_x}\right|\frac{\Delta\varepsilon_x}{\varepsilon_x} \tag{5.10}$$

where $\varepsilon_x$ is, according to the case at issue, the real or the imaginary part of $\varepsilon_w$ or $\varepsilon_s$.

To show results obtained from eq. (5.10), the error propagation factor $\dfrac{\varepsilon_x}{f(\mathbf{p})}\left|\dfrac{\partial f}{\partial \varepsilon_x}\right|$ is plotted,

see Figs.5-6, for HH polarization and different values of the orientation $\varphi$.

Let us first discuss the role of the real part of the dielectric constant, see Fig.5. In both Fig.5a

and Fig.5b plots describing the same entity, $\dfrac{\varepsilon_x}{f(\mathbf{p})}\left|\dfrac{\partial f}{\partial \varepsilon_x}\right|$, at variance of the orientation wall, are

reported. Fig.5a is particularized for the permittivity values typical of main building materials (dry

and aerated concrete, glass, bricks, wood) while Fig.5b focuses on the range of permittivity of the

most of grounds.

For every orientation, the most critical values of $\varepsilon_r$ (those for which $\dfrac{\varepsilon_x}{f(\mathbf{p})}\left|\dfrac{\partial f}{\partial \varepsilon_x}\right|>1$) are in the

range 1÷2.5 but, with $\varphi$ increasing, that interval becomes shorter. Also in this case, information on

facades materials can be simply got and, above all, this information must be obtained once for each

building and can be used for every further analysis on it. Different considerations should be

emphasized for the ground whose electromagnetic behaviour can change according to the season or

the weather and/or can vary in any unpredictable time in connection to some man-made activities.

Fortunately, the influence on height retrieval deriving from an imperfect knowledge of ground

permittivity is very small for any building orientation.

Moving to the imaginary part of the dielectric constant, see Fig.6, we find a better behaviour.

As a matter of fact, for every orientation and for every $\varepsilon_i$ (now, the plots for wall and ground are

joined together) the error propagation factor $\dfrac{\varepsilon_x}{f(\mathbf{p})}\left|\dfrac{\partial f}{\partial \varepsilon_x}\right|$ keeps always under the value 0.5 (worst

case for $\varphi = 40°$) but usually is much smaller.

Concerning the error induced by the dielectric constants when a different polarization is considered, we can assess that when using cross-polarised data, the error propagation factor

$\dfrac{\varepsilon_x}{f(\mathbf{p})}\left|\dfrac{\partial f}{\partial \varepsilon_x}\right|$ is, for any orientation (except for $\varphi = 0°$ in which the scattering coefficient is identically

null), similar to its counterpart in HH (even smaller for wall materials permittivity) while, in the VV

polarization, the same factor is quite always worsen than it is in the other polarizations.

Many other interesting discussions can be introduced on performances of the approach with respect

to other relevant parameters. However, our approach provides the complete mathematical

framework to start this new discussion and we do think that the interested reader, lead by the

analysis presented in the paper, and using equations provided in this Section can now carry on his

own studies on parameters of interest.

### 5.3 Model inaccuracy

Let us consider now the case in which the errors on the building height retrieval are caused

by approximations on the geometric model. The simple basic shape assumed for the building (i.e. a

parallelepiped) is improved in this Section by considering the presence of windows and balconies,

see Fig.7, in order to evaluate the errors committed in neglecting them.

At this aim the radar cross section is now written as

$$\sigma° = h \cdot l \cdot g(\mathbf{q}) \tag{5.11}$$

where $\mathbf{q} = (\sigma, L, \varepsilon_w, \varepsilon_s, \varphi, \vartheta)$ and $g(\mathbf{q}) \cdot l = f(\mathbf{p})$ previously introduced, so that (4.1) can be rewritten as

$$h = h_c \frac{\hat{\sigma}^{\circ}}{\hat{\sigma}_c^{\circ}} \frac{l_c g(\mathbf{q}_c)}{l\, g(\mathbf{q})} \quad . \tag{5.12}$$

Let us consider the presence of $n_w$ windows, represented as rectangular holes (it corresponds to the worst case in which all windows are open) of size $h_w * l_w$. In this case, the measured radar cross section is

$$\hat{\sigma}^{\circ} = (h \cdot l - A_w) \cdot g(\mathbf{q}) \quad , \tag{5.13}$$

where $A_w = h_w l_w n_w$ is the area occupied by windows. A similar expression holds for the calibrating building, for which subscripts $c$ for all variables are used.

If we ignore the presence of windows and use eq.(5.12) to retrieve the height, we obtain, substituting (5.13) in (5.12):

$$\hat{h} = h_c \frac{(hl - A_w)l_c}{(h_c l_c - A_{wc})l} = h \frac{1-x}{1-x_c} \quad \Rightarrow \quad \frac{\Delta h}{h} = \frac{\hat{h}-h}{h} = \frac{x - x_c}{1 - x_c} \quad , \tag{5.14}$$

where $\hat{h}$ is the estimated height, $x = \dfrac{A_w}{lh}$ and $x_c = \dfrac{A_{wc}}{l_c h_c}$ are the fractions of a façade occupied by windows in examined and calibrating buildings, respectively. Note that if the two buildings belong to the same part of the urban area (i.e., both are downtown, or in a residential area, and so on), these fractions are usually similar, and the height relative error is small.

A similar procedure can be used to analyse the effect of the presence of balconies. In this case, eqs.(5.13-14) can still be used if $A_w$ and $A_{wc}$ are replaced by $A_b$, and $A_{bc}$, which are the areas of wall that do not contribute to the mechanism of double reflection with the ground, for examined and calibrating building, respectively. These areas have different expressions for balconies with

reflecting banisters and transparent banisters at microwaves. In the latter case, see Fig.7a, we have $A_b = l_b \cdot \min\{2 s n_f, h\}$, where $l_b$ is the length of one balcony multiplied by the number of balconies in a floor, $n_f$ is the number of floors, $s = b/\text{tg}(\vartheta)$, and $b$ is the balcony depth. For reflecting banisters, see Fig.7b, $A_b = l_b \cdot \min\{(2 s + h_{bn}) n_f, h\}$, where $h_{bn}$ is the height of the banister, and $m' = b/tg(\theta)=s$, appearing in Fig.7b, is the portion of the wall above the banister contributing to the scattering of order greater than two. Accordingly, also in the presence of balconies we can state that if the two buildings belong to the same part of the urban area, then the height relative error is small. We can also note that the fraction of incident power that does not contribute to double scattering with ground, does contribute to multiple scattering from balconies, which corresponds to different returns placed in different range bins if the resolution is sufficiently high. These returns could be used for instance to count the number of floors of the building. However, this issue goes beyond the scope of the present paper and is not discussed here.

Finally, with regard to the effects of inaccuracies in the electromagnetic scattering model, a way to assess them is the application of the retrieval method to simulated images. An example is provided in the next Section.


### VI. Retrieval results

In order to test the procedure described in the previous section, we apply it to simulated SAR images that are able to provide us relevant and significant canonical cases with parameters of interest that can be fixed or changed in a controlled way.

SAR raw signals of different cases of isolated buildings on rough terrain have been simulated and processed, letting geometrical and electromagnetic parameters vary as well as the building orientation with respect to the sensor flight trajectory.

In Table III, geometrical and electromagnetic parameters regarding the scene described in Figure 8 are reported. The relevant simulated SAR image is shown in Fig.9. For this simulation

example, a frequency of 1.282 GHz and a radar look angle $\theta$ of 28° have been set. For roughness parameters involved (Tab.III), the GO solution has been considered for multiple scattering. The PO solution has been used, instead, for single scattering from the building wall and roof.

As we can see from Fig.8 and Table III, in this first example the same electromagnetic features and the same orientation of 20 degrees with respect to the radar flight trajectory have been considered for the three buildings in the scene; however, they have different heights.

In all simulations the presence of at least three buildings is considered, and we assume that we know the height of two of them in order to perform the calibration operation described in Section IV.

Let us assume that the calibrators for the scene at hand are the buildings located on the top and the bottom of the SAR image; then, we want to retrieve information on the height of the remaining central building. It is simple to verify that, being $\theta > \theta_p$ for the higher building in the top, this relation is also verified for the other buildings and, in particular, for the central one. So, both Eqs.(3.1), (3.2) can be applied for the height retrieval. Results of the building height retrieval from layover and shadow sizes are listed in the first two rows of Table IV, see Example n.1. The corresponding errors are also listed and evaluated as the difference between the retrieved height $h_e$ and the true one $h$.

Now, let us move to the building height extraction from the double reflection. For this method, the first step is to isolate, for each building, the double reflection contribution. After having collected all pixels interested by this contribution, the relevant grey levels are averaged and this mean value is directly proportional to the radar cross section (after the calibration operation) which is linked to the building height by eq.(3.8). The building height value retrieved according to the procedure described in Section IV from the double reflection contribution is listed in the last row of Table IV, see again Example n.1. This result is really interesting because it shows that the model-based procedure we propose for building height extraction from radiometric parameters performs much better than the building height extraction from geometric parameters (at least for the

considered scene and SAR system resolution). It should be noted that this could be partly due to the fact that the same electromagnetic model used in the simulation is also used in the inversion. However, results on real SAR images, reported in [2], seem to support the results obtained here from simulated images.

Let us consider a slightly different scene. In this case, as shown in the pictorial view of the scene in Fig.10 as well as in the relative SAR image in Fig.11, the buildings present different orientations with respect to the radar flight trajectory: from top to bottom, 30, 0 and 45 degrees of orientation are considered. The heights and the other parameters in the scene are left unchanged with respect to the Example n.1. Even if this situation is still canonical, it can be assumed that considering different orientations is surely more realistic and allows to better understand the potential of an application of this feature extraction approach to actual SAR images where, obviously, the buildings are not always aligned. Also in this case we get interesting results, see Example n.2 in Table IV. As we could expect, we exactly obtained the same results as in Example n.1 for the building height retrieved from layover and shadow (in fact, the geometric resolution is the same in the two examples). For the extraction from double reflection the result is different, even if very similar, because according to Eq.(3.8) a change in $\varphi$, left unchanged the height, produces a change in the double reflection contribution to the radar cross section and, consequently, a different distribution of the grey levels in the SAR image. Nevertheless, the result is still really promising.


## VII. Conclusions

In this paper a new model-based approach for parameter retrieval from SAR images of urban scenes has been presented. The general rationale has been explained, the limits and range of applicability have been shown and, above all, the important repercussions and potentiality in terms of applications have been highlighted.

The approach is based on a geometric and electromagnetic model of a built-up area. The influence of a not perfect (in actual cases) adhesion to the adopted model has been evaluated via an

error budget analysis. More complicated structures have been considered and the way they affect the retrieval scheme has been examined. In this context, a possible application has been illustrated, i.e. the building height retrieval from SAR images.

To carry on a complete sensitiveness analysis, simulated images have been considered. This study has shown that, in most cases, the relative error on the parameter to be retrieved becomes small by properly carrying on the calibration procedure. This justifies and generalises the good results obtained by applying the approach to actual images [1-2].

Some issues need to be further investigated.

Concerning the models, a  way to include more details in the geometric model, and consequently in the scattering one, without complicating too much the  set of equations, is under study; this would allow us to face those cases in which the  described approach is, at the present state, not applicable.

Moreover, this work suggests new matters to investigate. For example, the choice of the best SAR product (i.e., the best post-processing) represents one of the most urgent issues: present studies show that different methods and different applications require different product kinds.  The availability of new high resolution SAR images, as those provided by the sensors Cosmo SkyMed and TerraSAR-X, is driving the authors to rapidly deepen the matter.

**Appendix A**

In this Appendix we detail the "calibration operation" cited in Section IV. Due to the unknown attenuation and background additive noise, the measured radar cross section $\hat{\sigma}^o$ (i.e., the square of the SAR amplitude image grey level) corresponding to the double scattering contribution from a building of (unknown) height $h$ can be written as

$$\hat{\sigma}^o = A\sigma^o + B = A\,h\,f(\mathbf{p}) + B \quad,$$

(A.1)

where $\sigma^o$, $f(\mathbf{p})$ and $\mathbf{p}$ are defined in Section IV, and $A$ and $B$ are two unknown constants. The latter can be evaluated if the heights $h_b$ and $h_c$ of two buildings in the scene are known, together with the correspondent parameters $\mathbf{p}_b$ and $\mathbf{p}_c$. In fact, for these two "calibrating" buildings the measured double scattering radar cross sections are:

$$\hat{\sigma}_b^o = A\,h_b\,f(\mathbf{p}_b) + B$$

(A.2)

$$\hat{\sigma}_c^o = A\,h_c\,f(\mathbf{p}_c) + B \quad.$$

(A.3)

By solving the system of equations (A.2-3) with respect to the unknowns $A$ and $B$ we get

$$A = \frac{\hat{\sigma}_c^o - \hat{\sigma}_b^o}{h_c\,f(\mathbf{p}_c) - h_b\,f(\mathbf{p}_b)} \quad,\qquad B = \frac{h_c\,f(\mathbf{p}_c)\hat{\sigma}_b^o - h_b\,f(\mathbf{p}_b)\hat{\sigma}_c^o}{h_c\,f(\mathbf{p}_c) - h_b\,f(\mathbf{p}_b)} \quad.$$

(A.4)

By substituting (A.4) in (A.1) and solving (A.1) with respect to the unknown $h$, we get

$$h = \frac{h_c\,f(\mathbf{p}_c)\left(\hat{\sigma}^o - \hat{\sigma}_b^o\right) - h_b\,f(\mathbf{p}_b)\left(\hat{\sigma}^o - \hat{\sigma}_c^o\right)}{f(\mathbf{p})\left(\hat{\sigma}_c^o - \hat{\sigma}_b^o\right)} \quad.$$

(A.5)

If the additive constant is negligible, i.e., $B \cong 0$, then only one calibrating building is needed. In fact, in this case, from the ratio of (A.1) and (A.3) we get eq.(4.2).

**Appendix B**

In this Appendix we derive eq.(5.8).

If there is an error $\Delta s_{\mathrm{rms}}$ on the surface roughness, then the height is retrieved via (4.2), in which the function $f(\mathbf{p})$ is replaced by

$$f(\hat{\mathbf{p}}) = f(\mathbf{p}) \frac{\exp\left[-\dfrac{\tan^2 \vartheta \sin^2 \varphi}{2(s_{\mathrm{rms}} + \Delta s_{\mathrm{rms}})^2}\right]}{(s_{\mathrm{rms}} + \Delta s_{\mathrm{rms}})^2} \frac{s_{\mathrm{rms}}^2}{\exp\left[-\dfrac{\tan^2 \vartheta \sin^2 \varphi}{2 s_{\mathrm{rms}}^2}\right]} \tag{B.1}$$

and $f(\mathbf{p}_c)$ by $f(\hat{\mathbf{p}}_c)$, given by an expression analogous to (B.1). By using (B.1) and (A.1,3), with $B$=0, in (4.2), we obtain

$$\hat{h} = h \exp\left\{-\frac{\tan^2 \vartheta}{2}\left[\frac{1}{(s_{\mathrm{rms}} + \Delta s_{\mathrm{rms}})^2} - \frac{1}{s_{\mathrm{rms}}^2}\right]\left(\sin^2 \varphi_c - \sin^2 \varphi\right)\right\} \quad . \tag{B.2}$$

Finally, by letting $\dfrac{\Delta h}{h} = \dfrac{\hat{h} - h}{h} = \dfrac{\hat{h}}{h} - 1$ , we obtain eq.(5.8).

**References**

[1] R. Guida, A. Iodice, D. Riccio, U. Stilla, "Model-Based Interpretation of High-Resolution SAR Images of Buildings", *IEEE Journal of Selected Topics in Applied Earth Observations and Remote Sensing,* vol.1, no.2, pp.107-119, June 2008.

[2] R. Guida, G. Franceschetti, A. Iodice, D. Riccio, G. Ruello, and U. Stilla, "Building feature extraction via a deterministic approach: Application to real high resolution SAR images" *Proceedings of the International Geoscience and Remote Sensing Symposium,* pp.2681-2684, Barcelona, Spain, 2007.

[3] J.A.Benediktsson, M.Pesaresi, K.Arnason, "Classification and Feature Extraction for Remote Sensing Images From Urban Areas Based on Morphological Transformations", *IEEE Trans. Geosc. Remote Sensing*, vol.41, no.9, pp.1940-1949, Sept.2003.

[4] F.Dell'Acqua, P.Gamba, "Detection of urban structures in SAR images by robust fuzzy clustering algorithms: the examples of street tracking", *IEEE Trans. Geosc. Remote Sensing*, vol.39, no.10, pp.2287-2297, Oct.2001.

[5] F.Dell'Acqua, P.Gamba, G.Lisini, "Improvements to Urban Area Characterization Using Multitemporal and Multiangle SAR Images", *IEEE Trans. Geosc. Remote Sensing*, vol.41, no.9, pp.1996-2004, Sept.2003.

[6] P.Gamba, B.Houshmand, M.Saccani, "Detection and Extraction of Buildings from Interferometric SAR Data", *IEEE Trans. Geosc. Remote Sensing*, vol.38, no.1, pp.611-618, Jan.2000.

[7] M.Quartulli, M.Datcu, "Information Fusion for Scene Understanding From Interferometric SAR Data in Urban Environments", *IEEE Trans. Geosc. Remote Sensing*, vol.41, no.9, pp.1976-1985, Sept.2003.

[8] M.Quartulli, M.Datcu, "Stochastic Geometrical Modeling for Built-Up Area Understanding from a Single SAR Intensity Image with Meter Resolution", *IEEE Trans. Geosc. Remote Sensing*, vol.42, no.9, pp.1996-2003, Sept.2004.

[9] C. Tison, F. Tupin, and H. Maitre, "A fusion scheme for joint retrieval of urban height map and classification from high resolution interferometric SAR images," *IEEE Trans. Geosci. Remote Sens.*, vol. 45, no.2, pp. 496–505, Feb.2007.

[10] A. Thiele, E. Cadario, K. Schulz, U. Thoennessen, and U. Soergel, "Building recognition from multi-aspect high-resolution InSAR data in urban areas," *IEEE Trans. Geosci. Remote Sens.*, vol. 45, no.11, pp. 3583–3593, Nov.2007.

[11] A.J.Bennett, D.Blacknell, "The Extraction of Building Dimensions from High Resolution SAR Imagery", *Proceedings of the International Radar Conference 2003*, pp.182-187, 2003.

[12] R.Bolter, "Reconstruction of Man-Made Objects from High Resolution SAR Images", *IEEE Aerospace Conference Proceedings*, vol.3, pp.287-292, 2000.

[13] C.Tison, F.Tupin, H.Maitre, "Retrieval of building shapes from shadows in high resolution SAR interferometric images", *Proceedings of the International Geoscience and Remote Sensing Symposium,* pp.1788-1791, Toulouse (France), 2004.

[14] G.Franceschetti, R.Guida, A.Iodice, D.Riccio, G.Ruello, "Deterministic Extraction of Building Parameters from High Resolution SAR Images", *Proceedings of the 3rd  RSS/ISPRS joint Symposium on Remote Sensing and Data Fusion over Urban Areas,* Tempe (Arizona, USA), 2005.

[15] G.Franceschetti, R.Guida, A.Iodice, D.Riccio, G.Ruello "Models for feature extraction from SAR images of urban areas", *Proceedings of the XXVIII<sup>th</sup> URSI General Assembly,* New Delhi (India), 2005.

[16] G.Fornaro, F.Lombardini, F.Serafino, "Three-dimensional multipass SAR focusing: experiments with long-term spaceborne data", *IEEE Trans. Geosc. Remote Sensing*, vol.43, no.4, pp.702-714, April 2005.

[17] E. Simonetto, H. Oriot, R. Garello, "Rectangular building extraction from stereoscopic airborne radar images", *IEEE Trans. Geosci. Remote Sens.,*vol.43, n.10, pp.2386-2395, Oct.2005.

[18] F. Xu and Y.-Q. Jin, "Automatic reconstruction of building objects from multi-aspect metric-resolution SAR images," *IEEE Trans. Geosci. Remote Sens.,*vol.45, no.7 pp.2336-2353, Jul. 2007.

[19] F.Tupin, "Extraction of 3D information using overlay detection on SAR images", *Proceedings of the 2nd GRSS/ISPRS Joint Workshop on Remote Sensing and Data Fusion over Urban Areas,* pp.72-76, Berlin (Germany), 2003.

[20] V.Amberg, M.Coulon, P.Marthon, M.Spigai, "Structure extraction from high resolution SAR data on urban areas", *Proceedings of the International Geoscience and Remote Sensing Symposium,* pp.1784-1787, Toulouse (France), 2004.

[21] G.Franceschetti, A.Iodice, D.Riccio, "A canonical problem in electromagnetic backscattering from buildings", *IEEE Trans. Geosc. Remote Sensing*, vol.40, no.8, pp.1787-1801, Aug.2002.

[22] G.Franceschetti, A.Iodice, D.Riccio, G.Ruello "SAR raw signal simulation for urban structures", *IEEE Trans. Geosc. Remote Sensing*, vol.41, no.9, pp.1986-1995, Sept.2003.

[23] F.T.Ulaby, R.K.Moore, A.K. Fung, *Microwave Remote Sensing: Active and Passive, Vol. I -- Microwave Remote Sensing Fundamentals and Radiometry*, Addison-Wesley, Advanced Book Program, Reading, Massachusetts, 1981.

[24] La Prade, "Elevations from radar imagery", Photogrammetry Engineering,vol.35, p.366-371, 1969.

[25] C.R. Rao, H. Toutenburg, A. Fieger, C. Heumann, T. Nittner and S. Scheid, Linear Models: Least Squares and Alternatives, Springer Series in Statistics, 1999.

[26] T.Pavlidis, *Structural pattern recognition*, Springer-Verlag, 1977.

**Captions of Figures**

Fig.1: The geometric model adopted for the buildings in the scene.

Fig.2: Cut at constant azimuth of the scene; composition of different contributions in the SAR image is also displayed. *X* is the total range size of the area affected by the roof backscattering; $\vartheta$ is the SAR look angle.

Fig.3: Top view of the urban scene (*x-y* plane) and corresponding SAR image (*x-r* plane). Ground-slant range projection is also shown.

Fig.4: Plot of the error propagation factor $\dfrac{\Delta h}{h} \Big/ \dfrac{\Delta \varphi}{\varphi}$ at variance of $\varphi$ for different polarizations: HH, VV, HV.

Fig.5: Plot of the error propagation factor $\dfrac{\Delta h}{h} \Big/ \dfrac{\Delta \varepsilon_{wr}}{\varepsilon_{wr}}$ for HH polarization with $\varphi$ varying from

0° to 40° with step of 10°.

Fig.6: Plot of the error propagation factor $\dfrac{\Delta h}{h} \Big/ \dfrac{\Delta \varepsilon_{wi}}{\varepsilon_{wi}}$ for HH polarization with $\varphi$ varying from

0° to 40° with step of 10°.

Fig.7: Interaction between the radar signal and a building with balconies: (a) banisters

transparent at microwaves, (b) banisters reflecting at microwaves.

Fig.8: 3-D view of a canonical scene with building wall orientation of 20 degrees.

Fig.9: Simulated SAR image of the scene represented in Fig.8.

Fig.10: 3-D view of a canonical scene where building wall orientation is, from the top to

bottom, 30, 0 and 45 degrees.

Fig.11: Simulated SAR image of the scene represented in Fig.10.
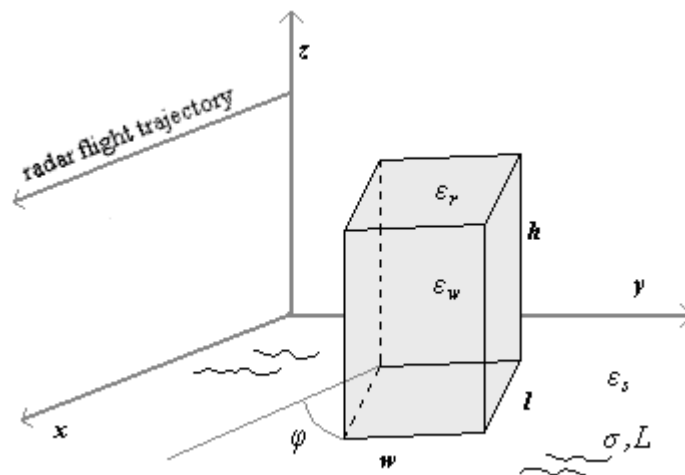


Figure 1
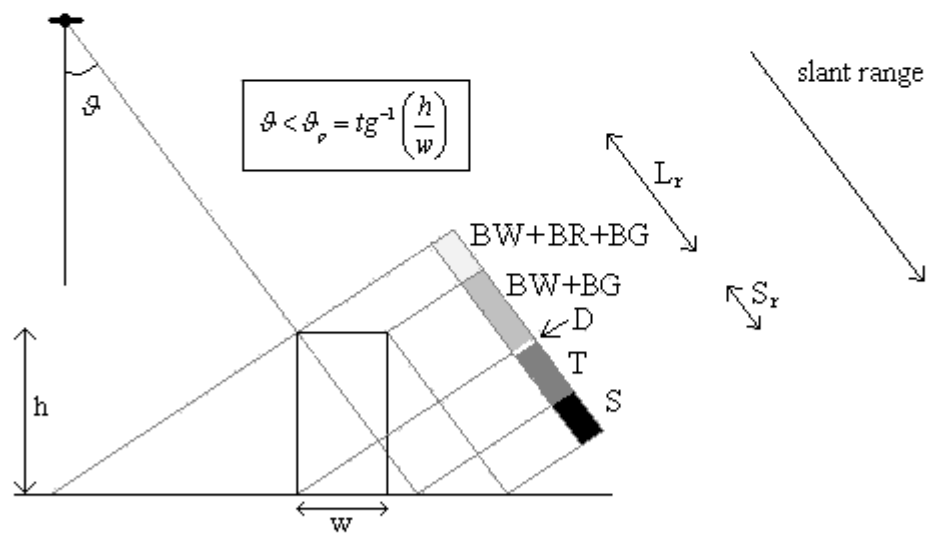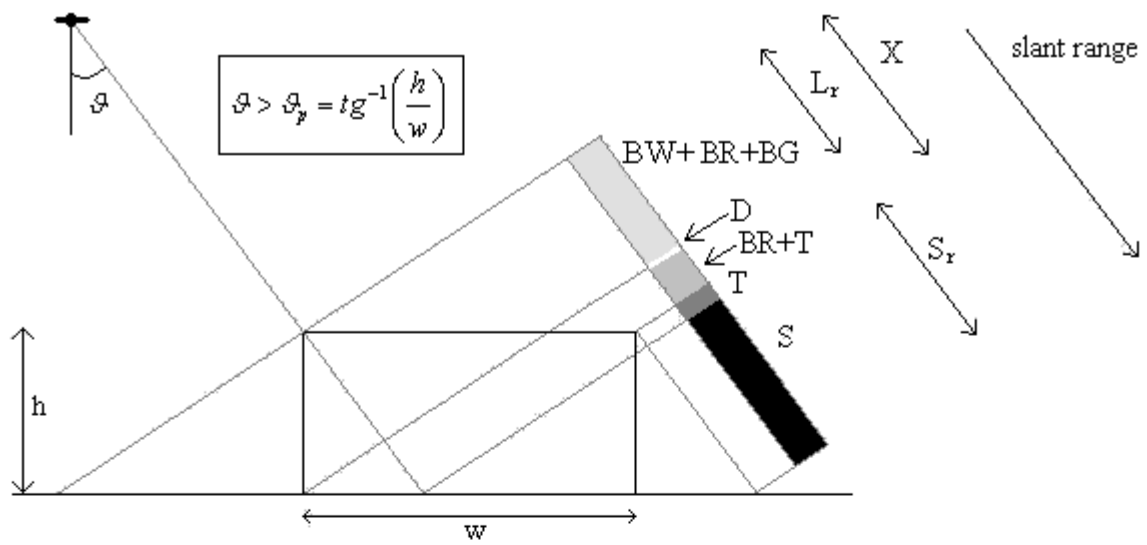
**Legenda**

BW = Backscattering from Wall
BR = Backscattering from Roof
BG = Backscattering from Ground
D = Double scattering

T = Triple scattering
Lr = Range size of Layover
Sr = Range size of Shadow
S = Shadow

Figure 2

$$dy = dr \cdot \cos\theta$$
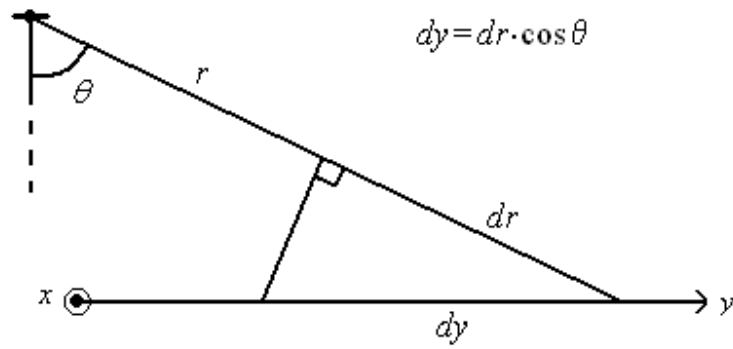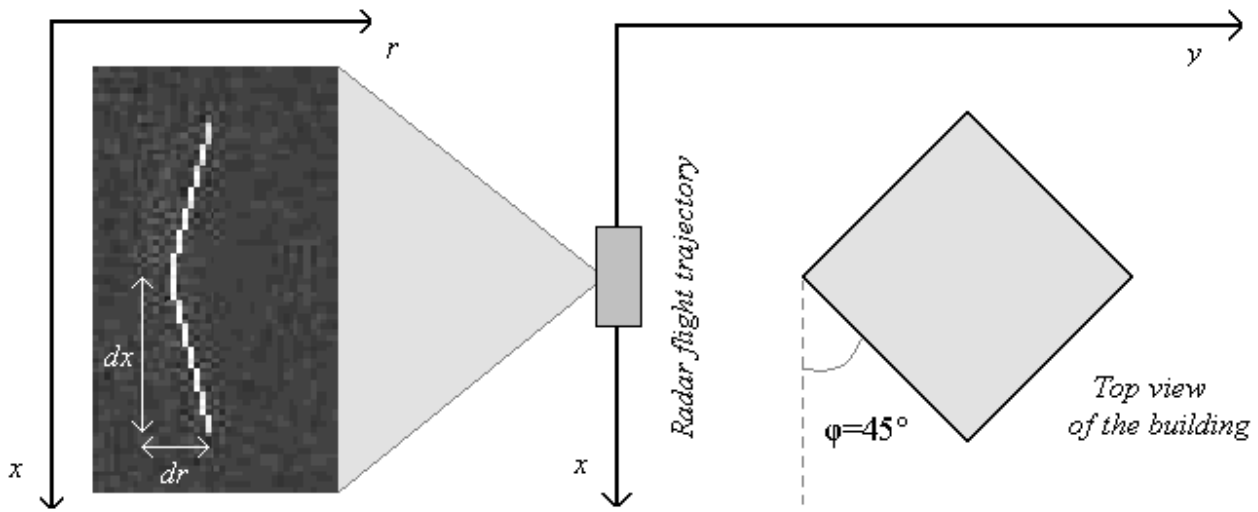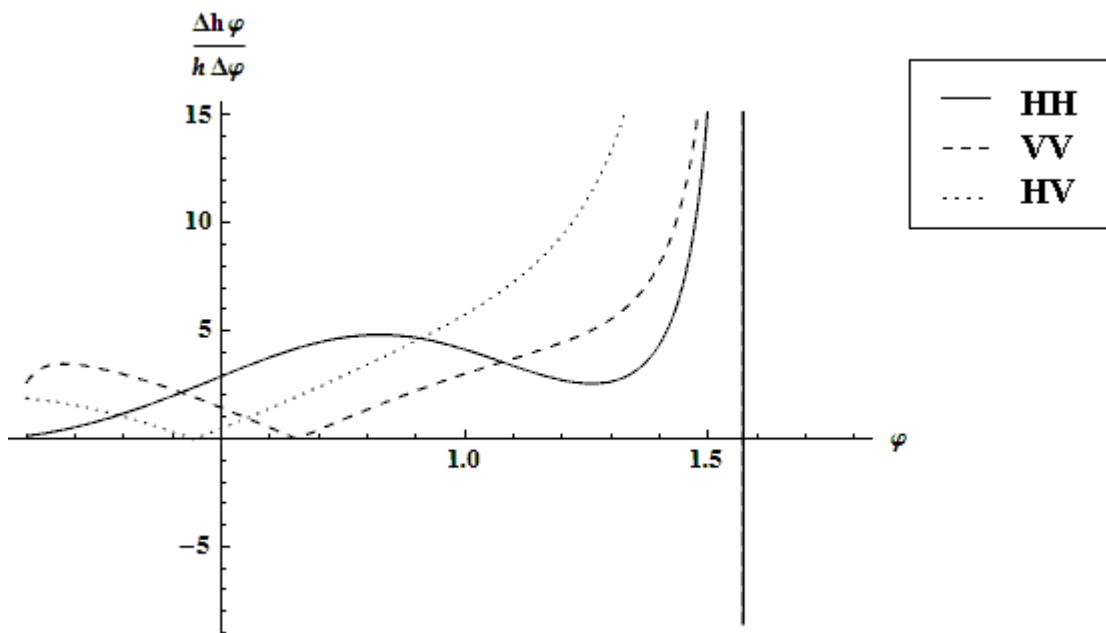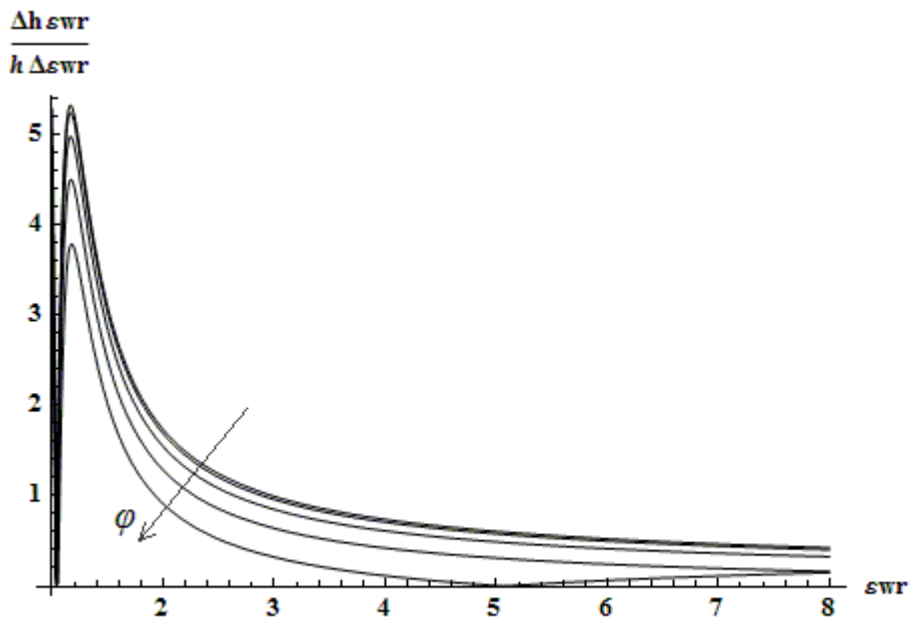
Figure 3



Figure 4

(a)



(b)

Figure 5

Figure 6



$$s = b/tg\theta = p$$

**(a)**

$$s = b/tg\theta = m'$$

**(b)**
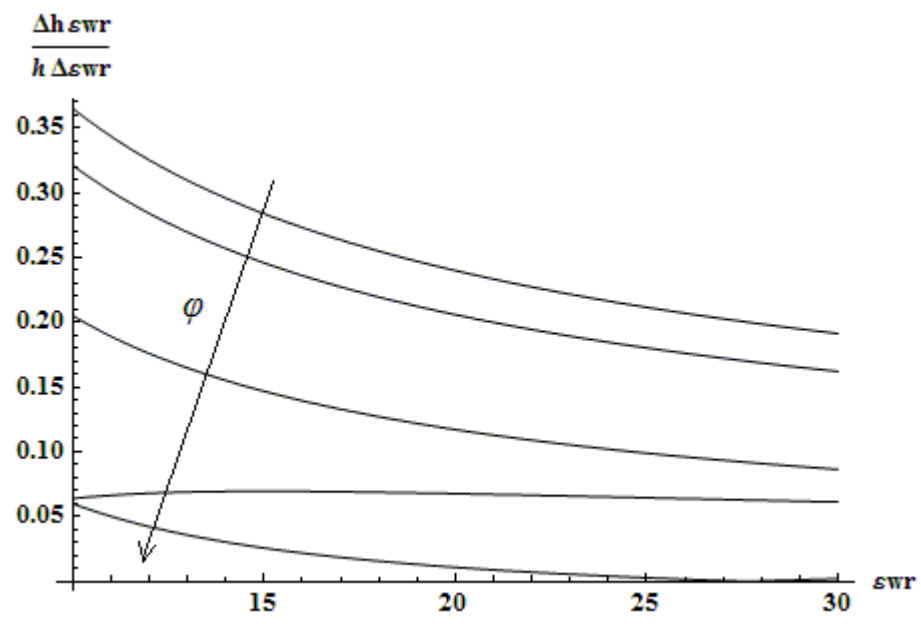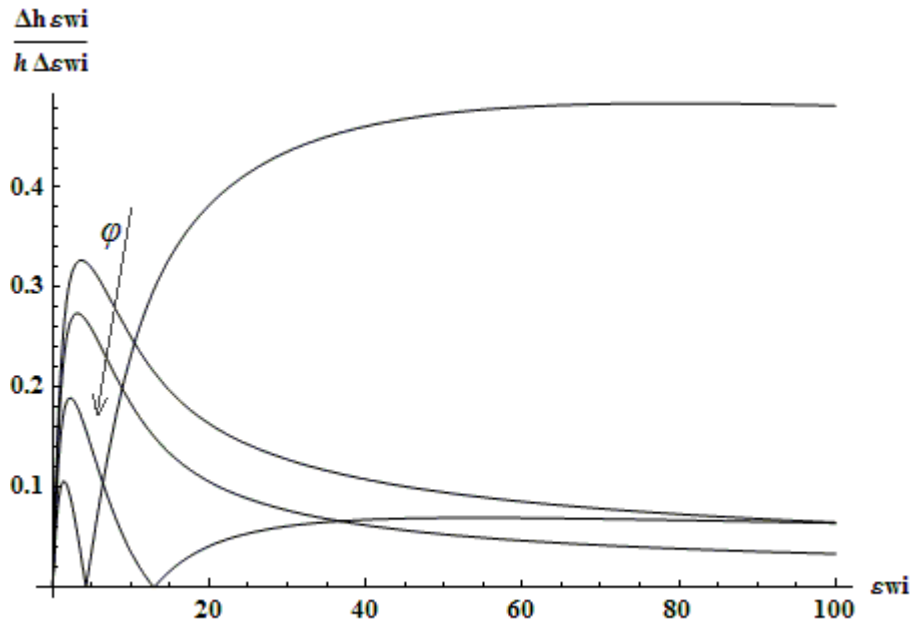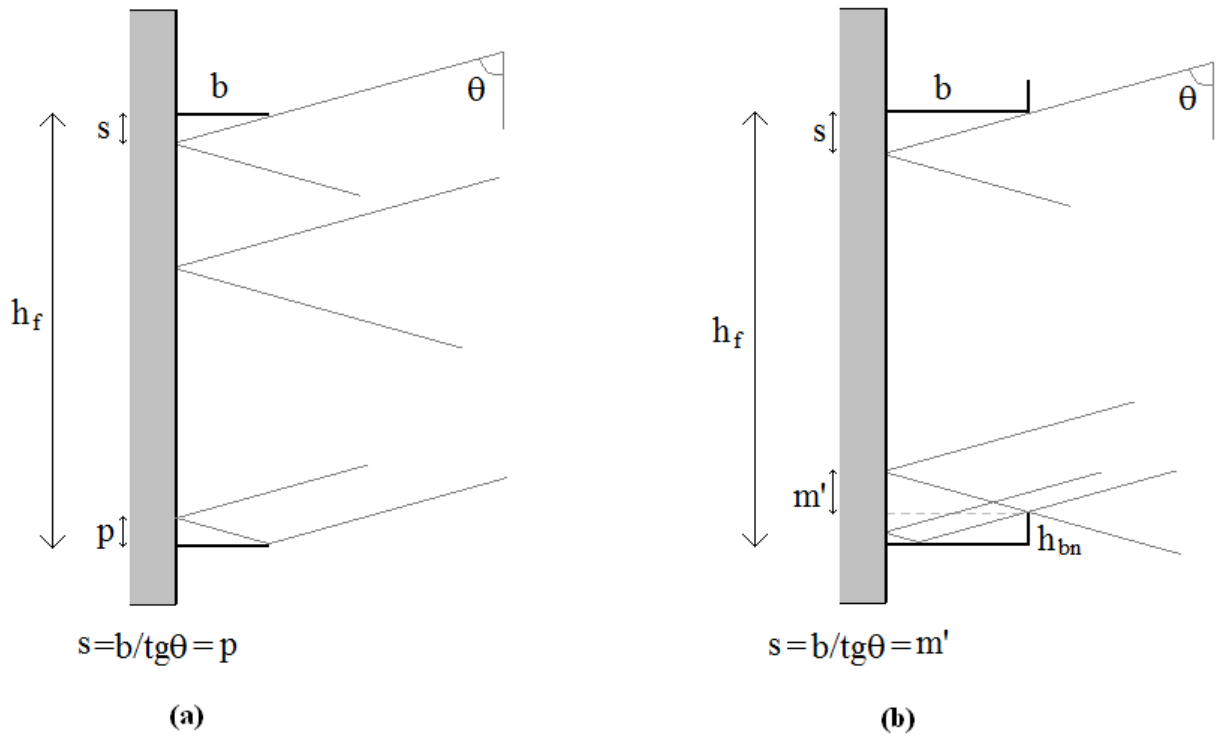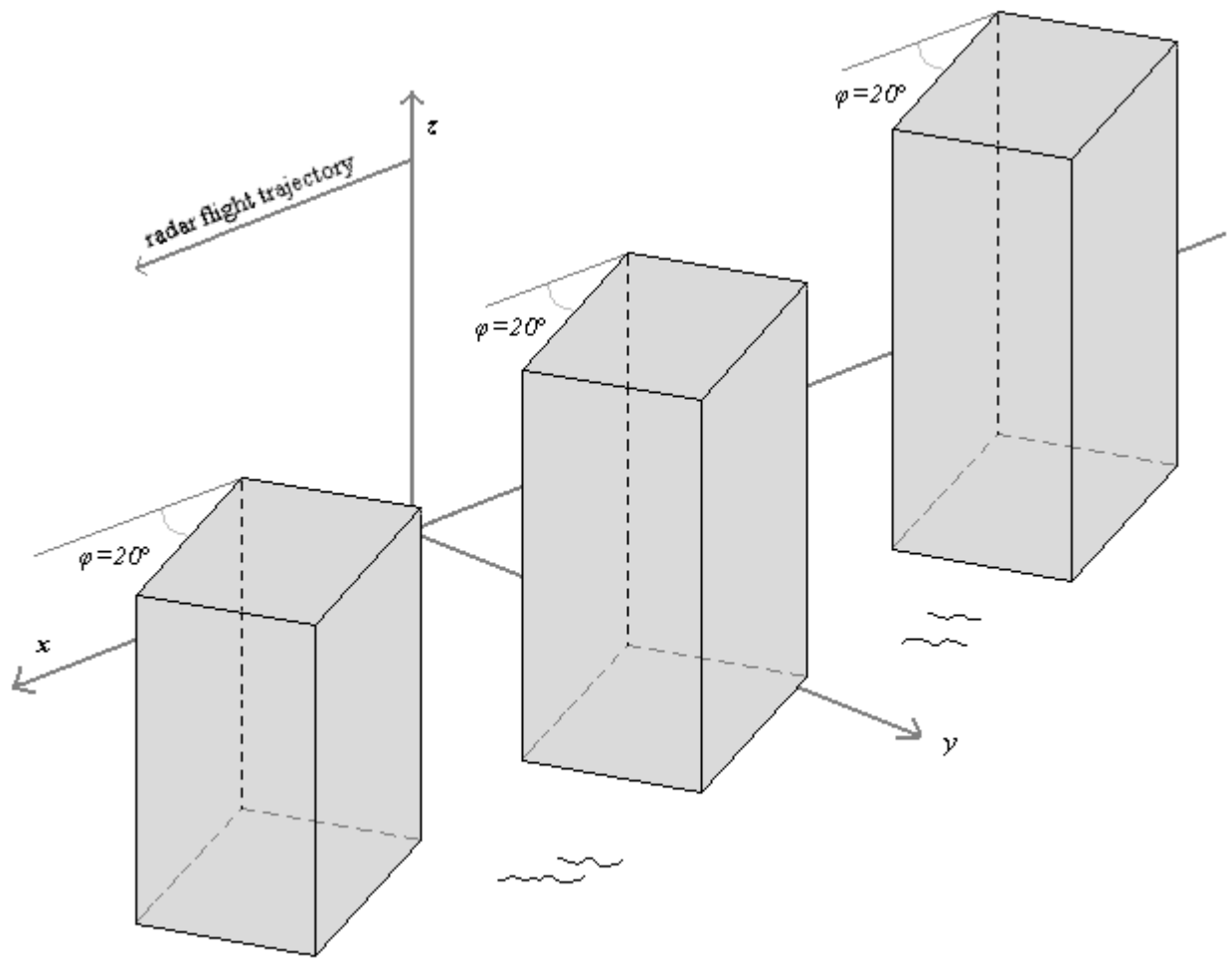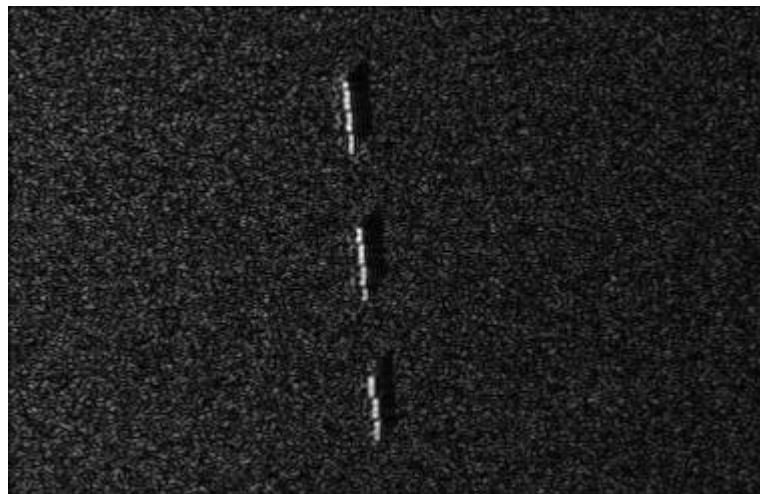
Figure 7

Figure 8



Figure 9
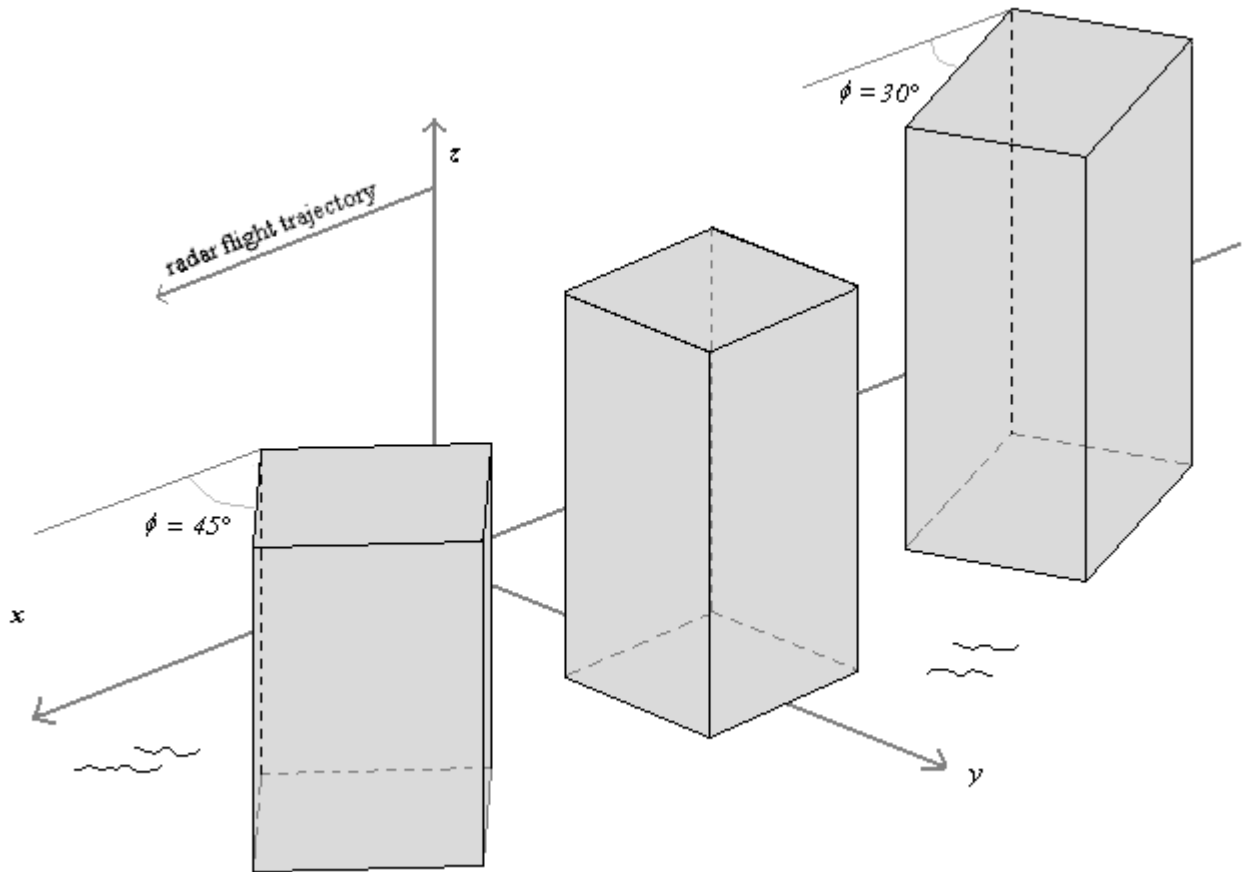
Figure 10
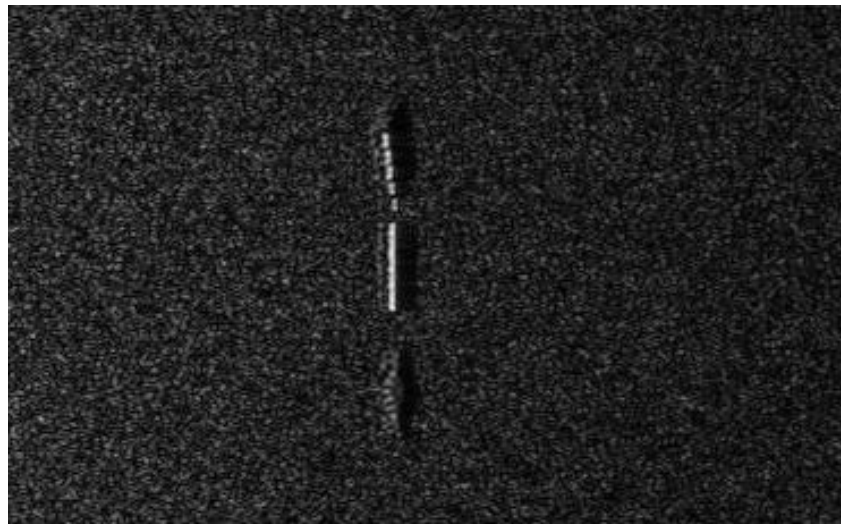


Figure 11

**Captions of Tables**

Table I: Relationships among geometrical parameters and those measurable on the SAR image.

Table II: Relationships among electromagnetic parameters and those measurable on the SAR image.

Table III: Geometric and electromagnetic parameters describing the scene considered in the simulation examples.

Table IV: Results of building height retrieval from simulated SAR images in Figs.9,11.

## Table I

| The building height *h* is linked to | The building length *l* is linked to | The building depth *w* is linked to | The angle *φ* is linked to | The roughness parameters $\sigma$ and *L* are linked to |
|---|---|---|---|---|
| • layover range size<br>• shadow range size<br>• radar cross section | • the shape of the building in the SAR image (particularly the azimuth extension of building image when φ=0)<br>• radar cross section | • the shape of the building in the SAR image (particularly, the range extension of single scattering from roof when φ=0) | • the shape of building image radar cross section | • radar cross section |
| through<br><br>▪ single scattering from wall<br>▪ double scattering<br>▪ triple scattering | through<br><br>▪ single scattering from wall<br>▪ double scattering<br>▪ triple scattering | | through<br><br>▪ single scattering from wall<br>▪ double scattering<br>▪ triple scattering; | through<br><br>▪ single scattering from ground<br>▪ double scattering<br>▪ triple scattering. |

## Table II

| The complex dielectric constant of building wall $\varepsilon_w$ is linked to | The complex dielectric constant of building roof $\varepsilon_r$ is linked to | The complex dielectric constant of building soil $\varepsilon_s$ is linked to |
|---|---|---|
| radar cross section through<br><br>• single scattering from wall<br><br>• double scattering<br><br>• triple scattering; | radar cross section through<br><br>• single scattering from roof | radar cross section through<br><br>• double scattering<br><br>• triple scattering |

## Table III

| | |
|---|---|
| Top building dimensions (length x width x height) | 100 m x 100 m x 45 m |
| Central building dimensions (length x width x height) | 100 m x 100 m x 40 m |
| Bottom building dimensions (length x width x height) | 100 m x 100 m x35 m |
| Roof and wall dielectric constant | 3 |
| Roof and wall conductivity | 0.01 S/m |
| Ground dielectric constant | 4 |
| Ground conductivity | 0.001 S/m |
| Ground standard deviation | 0.19 m |
| Ground correlation length | 1.54 m |
| Image resolution (slant range x azimuth) | 4.839 m x 2.571 m |

## Table IV

| Central building height estimations and errors | Example n.1 | | Example n.2 | |
|---|---|---|---|---|
| | Height *h* [m] | Error $e=h_e\text{-}h$ [m] | Height *h* [m] | Error $e=h_e\text{-}h$ [m] |
| from shadow | 42.73 | 2.73 | 42.73 | 2.73 |
| from layover | 32.89 | -7.11 | 32.89 | -7.11 |
| from double reflection | 38,60 | -1.40 | 38.63 | -1.37 |